Hindawi
Adsorption Science & Technology
Volume 2022, Article ID 5362178, 14 pages
https://doi.org/10.1155/2022/5362178

Research Article

Effect of Aging on the Adsorption of Tetracycline by Humic Acid: Insight into the Morphology and Chemical Composition

Chunli Zheng,[1,2] Fei He,[1] Zhiwu Cao,[3] Xingxing Cheng,[4] and Zhenxing Wang[5,6]

[1]*Department of Environmental Science and Engineering, School of Energy and Power Engineering, Xi'an Jiaotong University, Xi'an 710049, China*
[2]*Key Laboratory of Subsurface Hydrology and Ecological Effect in Arid Region of the Ministry of Education (Chang'an University), Xi'an 710049, China*
[3]*Bureau of Scientific and Technological Innovation, Transformation, and Promotion, Yangling Agricultural Hi-Tech Industries Demonstration Zone, Yangling 712100, China*
[4]*School of Urban Construction and Environment, Dongguan Key Laboratory of Green Energy, City College of Dongguan University of Technology, Dongguan 523419, China*
[5]*South China Institute of Environmental Sciences, MEE, Guangzhou 510655, China*
[6]*State Environmental Protection Key Laboratory of Water Environmental Simulation and Pollution Control, Guangzhou, 510655, China*

Correspondence should be addressed to Zhenxing Wang; 271886581@qq.com

Received 21 February 2022; Revised 25 June 2022; Accepted 17 August 2022; Published 10 October 2022

Academic Editor: Chinenye Adaobi Igwegbe

Tetracycline (TC) is a commonly used antibiotic and enters the soil environment continuously. As humic acid (HA) is one of the most important components in soils, it is necessary to investigate the adsorption behavior of TC by HA under different conditions. In this paper, the factor of "aging" was considered. The methodology of coating $CaCO_3$ precipitation on the surface of HA was adopted to simulate the aging process. The adsorption kinetics and isotherm demonstrated that the uptake of TC over HA was quicker with more amount than aged HA, meaning that aging affected the mass transfer of TC from the bulk solution to the outer surface of HA as well as from HA outer surface to its interior pores. To explain the effect of aging, BET was utilized to characterize the morphology of HA and aged HA. It was found that aging resulted in a decrease in specific surface area and pore size. XPS, FTIR, and 2D-COS revealed how aging influenced the chemical composition of HA. Five kinds of functional groups carried by HA contributed to the adsorption of TC, in which the binding affinity towards TC followed the order of –COO > N – H > –C – C > C – O > O – H. These results indicated that -COO was the most sensitive adsorption site. Compared to HA, the content of -COO for aged HA decreased obviously. In summary, aging affected the morphology and chemical position of HA and consequently lead to the change in adsorption kinetics and isotherm of TC.

1. Introduction

Antibiotics are widely used in human medicine and animal husbandry as they can inhibit the growth and reproduction of bacteria [1]. In 2013, the total antibiotic usage in China was approximately 162000 tons, 150 times high than in the UK, and the total production was estimated to be 248000 tons. It was reported that during the use process 54% of antibiotics would enter into soils [2].

The migration and transformation pathways of antibiotics in soils mainly include adsorption by soil particles, absorption by plants, and transportation by runoff. Its well-known adsorption is the key behavior that influences the ultimate fate of antibiotics in soils [3]. The physical and chemical properties

of soils such as organic matter, minerals, pH, and moisture affect the adsorption behavior. Among these factors, it is generally believed that organic matter is essential for the adsorption of organic pollutants by soils [4]. Humic acid (HA) is one of the most important components of organic matter. As it contains various functional groups such as hydroxyl, carboxyl, and carbonyl; HA can bind with antibiotics [5]. Vaz et al. [6] extracted HA from a kind of Brazilian soil according to the procedure suggested by the International Humic Substances Society (IHSS) and described the sorption mechanism of oxytetracycline (OTC) on HA. It was found that OTC interacted with the carboxyl group carried by HA, which enhanced the retention degree of OTC in the soil, therefore, the leaching of OTC to the groundwater was impeded. Gu et al. [7] also observed the complex interaction between tetracycline and the carboxylic group of HA.

In recent years, more and more studies reported the phenomenon of "aging" that happened in HA in nature [1, 8, 9]. Here, aging means the physical and chemical properties of HA changed with time [10–12]. For example, See and Bronk [13] found an increase in O-H and N-H functional groups carried by humic acid during one year period. Yu et al. [9] pointed out that since the properties of HA change, the adsorption behavior of pollutants correspondingly was affected. Therefore, it is necessary to investigate the influence of "aging" on the adsorption of antibiotics by HA. Till now, the studies that related to preparing "aging" samples mainly consider the factor of time scale. Reeves et al. [14] prepared the aged soil by storing the fresh soil in a stable system for a time scale of 270 d, and then the soil-bound organic pollutants availability was evaluated by in vivo and in vitro measurements. Guthrie et al. [15] prepared the aged sediments by storing the fresh sediments in dark in a 0.05% NaN_3 solution for a time scale of 120 d, in which the effect of aging on pyrene transformation and pyrene association with fractions of the sedimentary organic matrix was revealed. Besides the factor of time scale, aging also results from the superficial geochemical process such as precipitation. In the laboratory, scientists usually use the method of coating calcium salt precipitation on the surface of HA or soils to simulate the aging process [16, 17]. The adsorption performance of aged samples is generally investigated from a macroviewpoint, that is, only obtaining the adsorption kinetic and isotherm parameters. However, the exploration of mechanism from a microviewpoint was necessary such as the molecular interaction between the aged samples and target pollutants.

In this paper, $CaCO_3$ was used to wrap HA which was extracted from the soil sample based on the method provided by the International Humic Substances Society (IHSS). Tetracycline (TC) was selected as the pollutant as it is one of the most commonly used antibiotics [18]. This paper was helpful to understand the difference in the structure and chemical composition resulting from aging as well as the difference in the TC adsorption behavior brought about by aging.

2. Materials and Methods

2.1. Soil Sample and Chemicals. The soil samples were collected from the surface of 1-10 cm in an arable field located in the Qinling Mountains (109°15′ 36″ E, 33 °55′ 12″ N), Shaanxi Province, China. The fresh soil samples were dried naturally, sieved through a mesh (<2 mm), and preserved in a bottle under -4°C. The physiochemical properties of the soil samples were measured in our previous work [19]. Tetracycline hydrochloride (TC, purity > 98%) and NaOH (purity > 99%) were purchased from Dr. Ehrenstorfer (Germany). $CaCl_2$ (purity > 96%) and $NaCO_3$ (purity > 98%)were bought from Tianjin TianLi Chemical Reagent Ltd. (China). HCl solution (*w*/*v*, 38%) and HF solution (*w*/*v*, 40%) were of analytical grade and provided by J&K Scientific Ltd. (Shanghai, China). Ultrapure water was prepared by an ultrapure water instrument (ULUPURE, Sichuan Province, China). N_2 (purity > 99%) was bought from Xian TaiDa Cryogenic Equipment Ltd. (China).

2.2. Preparation of HA and Aged HA. The extraction of humic acid (HA) was operated according to the method provided by the International Humic Substances Society [6]. One hundred grams of the soil samples and 250 mL ultrapure water were mixed in a 500 mL conical flask, and then 1 mol/L of HCl was added until the pH of the mixture reached 1.5. 150 milliliters of HCl with 0.1 mol/L was poured into the 500 mL conical flask. The conical flask was placed in a shaker (Zhicheng, Shanghai, China) at 160 rpm and 25°C for 2 h, and then centrifuged (Xiangyi, Hunan, China) at 3000 rpm for 15 min to remove the supernatant. The pH value of the residual sediment was adjusted to be 7.0 with 1 mol/L of NaOH. Under the protection of nitrogen, 400 ml of NaOH with 0.1 mol/L was added and shaken for 24 hours at 25°C. The flask was centrifuged at 8000 rpm and 25°C for 15 min to collect the supernatant. The pH value of the supernatant was adjusted to be 1.0 with 6 mol/L HCl. Finally, the acidified supernatant was allowed to stand for 24 hours and then centrifuged at 3000 rpm and 25°C for 15 min. After discarding the supernatant, the sediment was freeze-dried at -60°C for 24 hours and named HA (Boyikang, Beijing, China).

HA aging was operated based on the method described by An et al. [16] 0.5 g of HA was placed into a 100 mL beaker and mixed with 20 mL of $CaCl_2$ solution with different initial concentrations (0.05 and 0.1 mol/L), respectively. All the beakers were shaken in dark for 24 hours at 25°C and 120 rpm. Twenty milliliters of $NaCO_3$ with 0.05 and 0.1 mol/L were correspondingly added to the beakers and shaken for 48 h to generate $CaCO_3$ precipitation on the surface of HA. The beakers were centrifuged at 8000 rpm and 25°C for 15 min to remove the supernatant. For cleaning the excess calcium carbonate, twenty milliliters of ultrapure water were used, and the cleaning process was repeated five times. Subsequently, the aging samples were obtained and freeze-dried. The two samples were named AHA-0.05 and AHA-0.1, respectively. HA, AHA-0.05, and AHA-0.1 were analyzed by BET, FT-IR, and XPS.

2.3. Adsorption Experiments. 1.2 g of $CaCl_2$ was mixed with ultrapure water in a 1000 ml volumetric flask to obtain 0.01 mol/L of $CaCl_2$ solution. 0.5 g of TC was dissolved in $CaCl_2$ solution (0.01 mol/L) and then placed in a 500 ml

volumetric flask to obtain TC stock solution with 1000 mg/L. The testing TC solutions with different concentrations were prepared by diluting TC stock solution with 0.01 mol/L of $CaCl_2$.

Adsorption kinetics: 0.2 g of HA, AHA-0.05, and AHA-0.1 was placed into a 50 mL plastic centrifugal tube, respectively, in which 30 mL of TC testing solutions with 20 mg/L was added. All the tubes were sealed by parafilm and shaken under 120 rpm and 25°C. Samples were withdrawn by a 5 mL pipette periodically and then centrifuged at 8000 rpm and 25°C for 5 min to collect the supernatant. The supernatant was filtered through a 0.45 μm membrane (GreenUnion, Jiangsu, China) and analyzed by a UV-Visible spectrophotometer (SP-1915, Spectrum, Shanghai, China) at the wavelength of 355 nm for determining the residual concentration of TC [20]. The calibration curves for TC are as follows: $y = 0.0324x + 0.0307$ ($R^2 = 0.997$), in which y stands for the absorbing intensity of spectroscopy and x for the concentration of TC. For calculating the adsorption amount q_t (mg/g), the equation is as follows:

$$q_t = V(C_0 - C)/M, \tag{1}$$

where C_0 is the initial concentration of TC (mg/L) in the solution, and C is the residual concentration (mg/L) at time t. V and M are the volumes of TC solution (L) and the mass of sorbent (g), respectively.

Adsorption isotherm: 0.2 g of HA, AHA-0.05, and AHA-0.1 was placed into a 50 mL plastic centrifugal tube, respectively, in which 30 mL of TC with different concentrations (5, 10, 20, 30, 40, and 50 mg/L) was added. All the tubes were sealed by parafilm and shaken under 120 rpm and 25°C. Samples were withdrawn by a 5 mL pipette after 24 h and then centrifuged at 8000 rpm and 25°C for 5 min to collect the sediment. The sediment was freeze-dried and then analyzed by FT-IR.

All experiments were performed three times and the mean value was used. For the control, each adsorbent was mixed with 0.01 mol/L of $CaCl_2$ solution and operated under identical conditions as mentioned above. The pseudo-first-order kinetic model Equation (2), the pseudo-second-order kinetic model Equation (3), and the Weber and Morris intraparticle diffusion model Equation (4) were used to calculate the kinetic parameters.

$$\mathrm{In}\left(q_{e,\exp} - q_t\right) = \mathrm{In}\left(q_{e,\mathrm{cal}}\right) - K_1 t, \tag{2}$$

$$\frac{t}{q_t} = \frac{1}{K_2 q_{e,cal}^2} + \frac{1}{q_{e,cal}} t, \tag{3}$$

where $q_{e,\exp}$ and q_t (mg/g) are the adsorption amount at equilibrium and time t, respectively. K_1 is the rate constant of the pseudo-first-order sorption (min^{-1}); K_2 is the rate constant of the pseudo-second-order sorption (g/(mg min)).

$$q_t = K_{id} t^{1/2} + I, \tag{4}$$

where q_t (mg/g) is the adsorption amount (mg/L) at any time t; K_{id} is the rate constant of the intraparticle diffusion model (mg/g.$min^{1/2}$). I (mg/g) is the intercept, related to the thickness of the boundary layer.

The Boyd's film-diffusion model shown in Equation (5) was used to determine the real control step related to the adsorption process of TC.

$$F(t) = 1 - \left(\frac{6}{\pi^2}\right) \sum_{n=1}^{\infty} \left(\frac{1}{n^2}\right) \exp\left(-n^2 B_t\right), \tag{5}$$

where $F(t) = q_t/q_e$ is the fraction of TC adsorbed at time t and equilibrium time. B_t is a function of $F(t)$. If $F(t)$ values is higher than 0.85.

$$B_t = 0.4977 - \ln(1 - F(t)). \tag{6}$$

If $F(t)$ values is lower than 0.85,

$$B_t = \left(\sqrt{\pi} - \sqrt{\pi - \left(\frac{\pi^2 F(t)}{3}\right)}\right)^2. \tag{7}$$

Two isotherm models, Freundlich and Dubinin-Radushkevich were employed.

$$q_e = K_F C_e^{1/n},$$
$$\ln q_e = \ln q_D - \left(\frac{R \bullet T}{\sqrt{2E}}\right)^2 \bullet \left(\ln\left(1 + \frac{1}{Ce}\right)\right)^2, \tag{8}$$

where Ce is the residual concentration of sorbate at equilibrium (mg/L); q_e is the uptake of sorbate on per unit mass of sorbent (mg/g); K_F (mg/$L^{(1-1/n)}$·g) and n are the Freundlich constants, which represent the adsorption capacity and intensity, respectively. q_D (mg/g) is the Dubinin–Radushkevich monolayer adsorption capacity. R is the gas constant (8.314 kJ/mol), and E is the mean free energy (kJ/mol).

2.4. Analysis. The porous structure of HA, AHA-0.05, and AHA-0.1 was measured by a physisorption analyzer (ASAP-2020, Micromeritics, Beijing) at 77 K. The pore size distribution was calculated by the Barrett-Joyner-Halenda (BJH) methods [21]. Scanning Electron Microscopy (SEM, TM-1000, Hitachi, Japan) was used to observe the detailed surface microstructure of HA, AHA-0.05, and AHA-0.1. X-ray photoelectron spectroscopy (XPS) of samples was recorded through Thermo Fisher ESCALAB Xi + via equipping an Mg Kα X-ray source (1253.6 eV protons). Before measurement, the HA and AHA were vacuum desiccated at -60°C for 24 h. The calibration values of O, N, and S were calibrated according to the calibration value of carbon at 284.6 eV. The functional groups of HA and AHA were characterized by Fourier Transform Infrared Spectroscopy (FT-IR) (Nicolet NEXUS 750, USA) with the KBr pellet method and the scanning spectra ranged from 500 to 4000 cm^{-1}. The resolution was 4 cm^{-1}. The FT-IR spectra were analyzed by two-dimensional correlation spectroscopy (2D-COS) as described by [22].

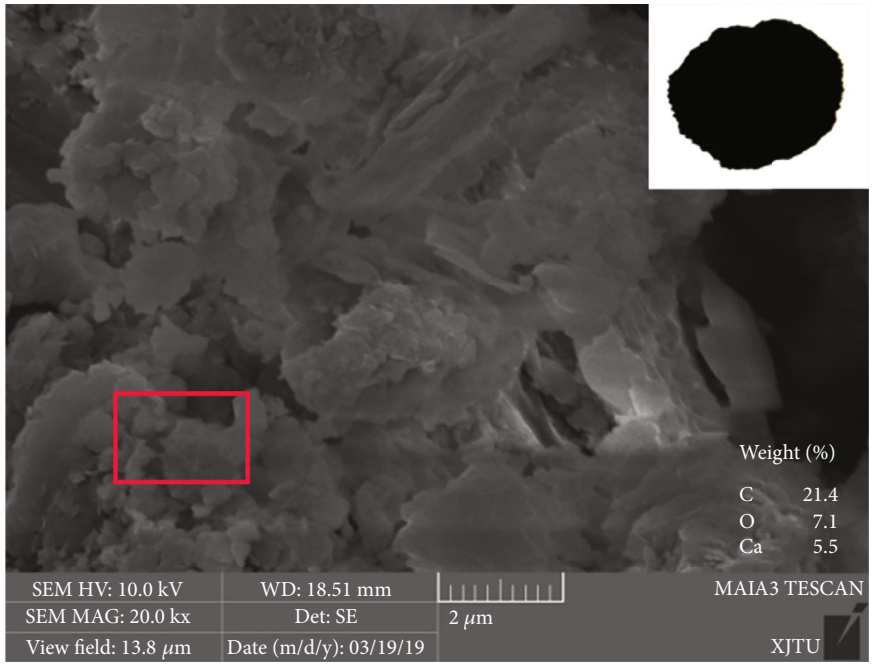

(a)

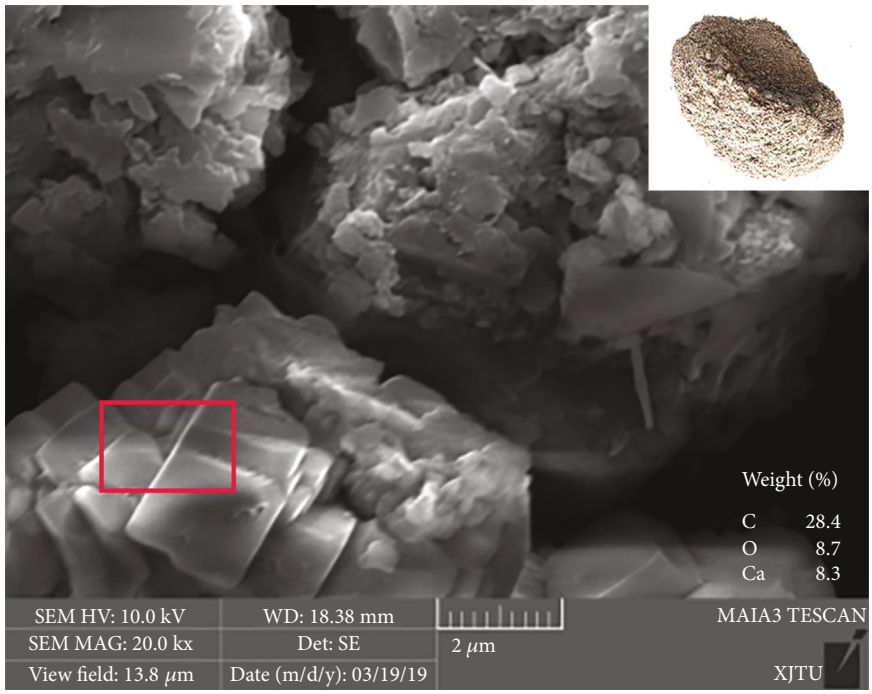

(b)

Figure 1: (a) SEM image of HA: insert is the outlook of HA; (b) SEM image of AHA: insert is the outlook of AHA.

3. Results and Discussion

3.1. Characterization of HA and AHA. As shown in the inserts of Figures 1(a) and 1(b), the extracted HA (named as HA) was black in color, and the HA after being treated with 0.1 mol/L of $CaCO_3$ (named as AHA) was charcoal gray. The reason for the color change might be the formation of white $CaCO_3$ deposits. The SEM images (Figures 1(a) and 1(b)) exhibited that HA was of aggregated and irregular structure (in red frame) while AHA was composed of massive particles. On the surface of AHA, a kind of regular block (in red frame) was observed, presumably attributing to calcium carbonate. EDS analysis demonstrated the weight percentage of Ca on the surface of HA was 5.5% while increased to 8.3% for AHA (Figures 1(a) and 1(b)), respectively. A similar phenomenon was found for oxygen

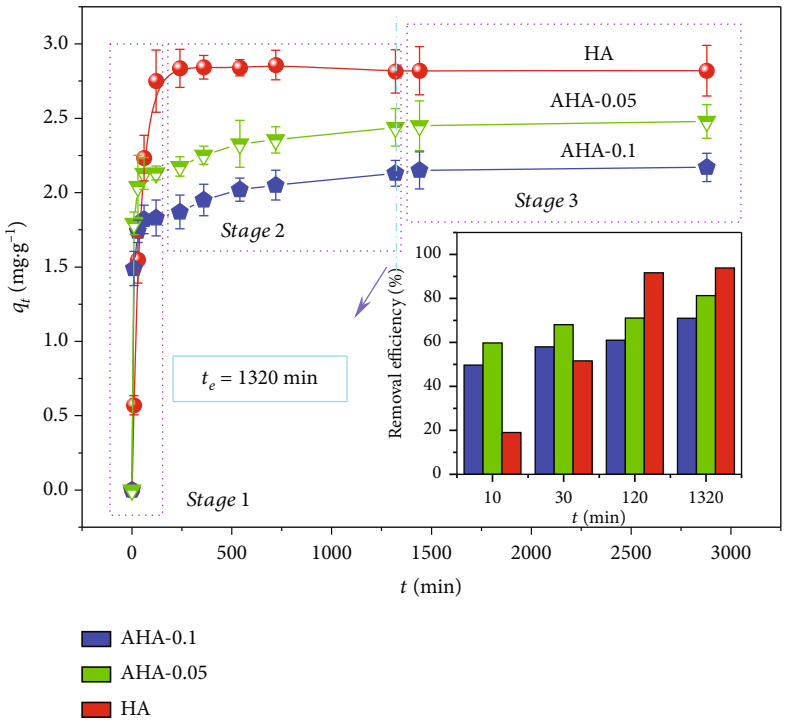

(a)

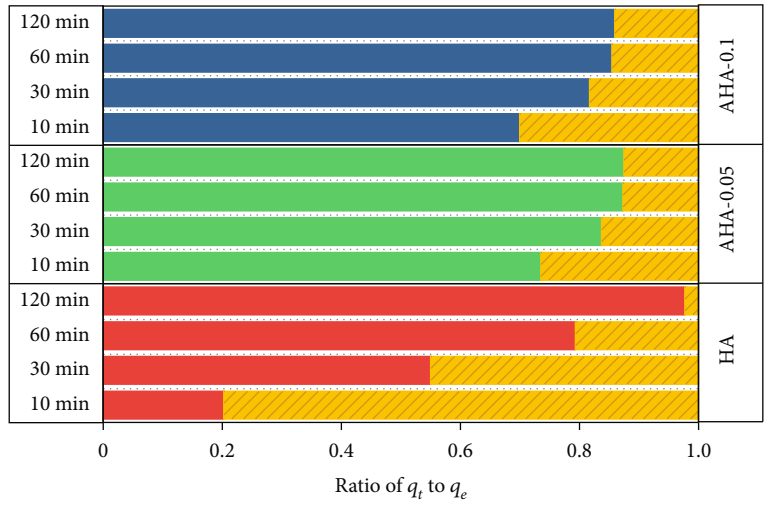

(b)

Figure 2: Continued.

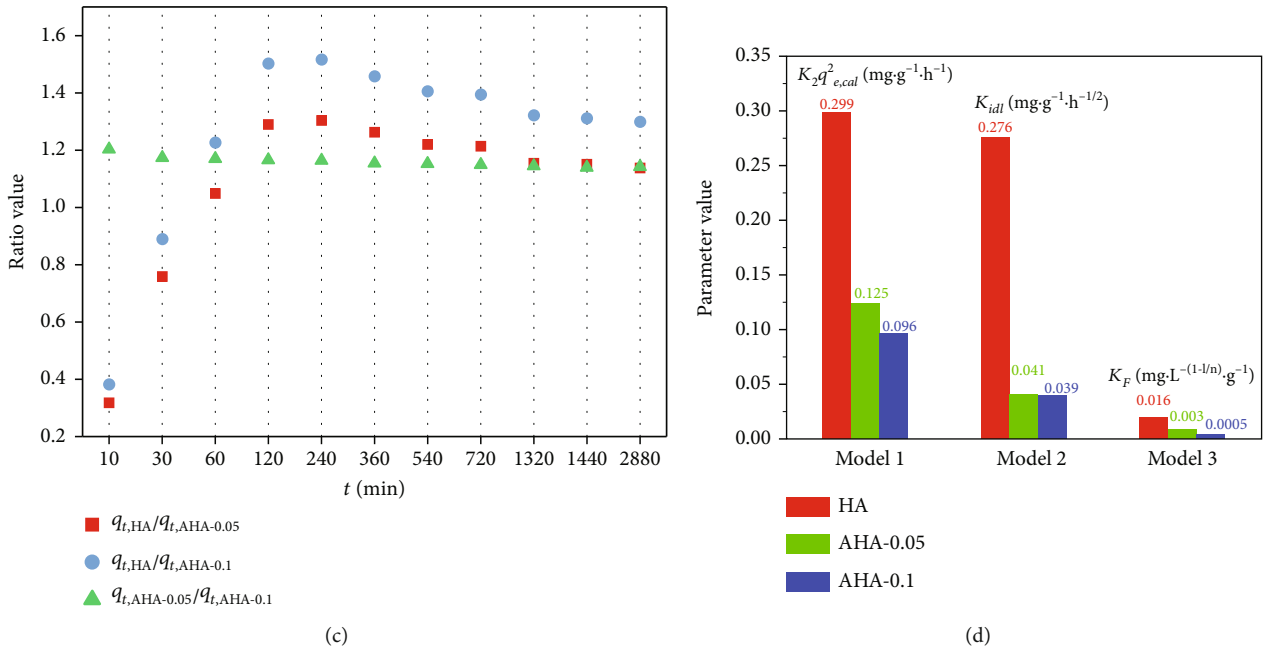

Figure 2: (a) Effect of contact time on the adsorption of TC in which the initial concentration was 20 mg/L (insert is the removal efficiency of TC under different contact time); (b) ratio of q_t to q_e under different contact time; (c) ratio of q_t between two different adsorbents; (d) the parameters of different models (model 1: pseudo-second-order model; model 2: Weber and Morris intraparticle diffusion model; model 3: Freundlich model).

Table 1: Parameters of the kinetic models for the adsorption of TC by HA and AHA samples.

Models	Parameters	HA	AHA-0.05	AHA-0.1
Pseudo-first-order				
	$q_{e,exp/}$mg·g^{-1}	2.82	2.48	2.17
	$q_{e,cal/}$mg·g^{-1}	1.383	1.274	1.139
	$K_{1/}$h^{-1}	0.0005	0.001	0.001
	R^2	0.852	0.827	0.831
Pseudo-second-order				
	K_2/g·mg^{-1}·h^{-1}	0.037	0.02	0.02
	$q_{e,cal/}$mg·g^{-1}	2.841	2.488	2.197
	R^2	0.999	0.999	0.992
	$K_2q^2_{e,cal/}$mg·g^{-1}·h^{-1}	0.299	0.125	0.096
Weber and Morris intraparticle diffusion				
	$Ki_{d1/}$mg·g^{-1}·h$^{-1/2}$	0.276	0.041	0.039
	I_1/mg·g^{-1}	-0.115	1.493	1.742
	R^2	0.944	0.923	—
	$Ki_{d2/}$mg·g^{-1}·h$^{-1/2}$	0.0004	0.0085	0.0860
	$I_{2/}$mg·g^{-1}	2.8100	2.0850	1.7830
	R^2	0.831	0.650	—
Boyd's film-diffusion model				
	Intercept	-0.702	0.906	0.845
	R^2	0.955	0.744	0.648

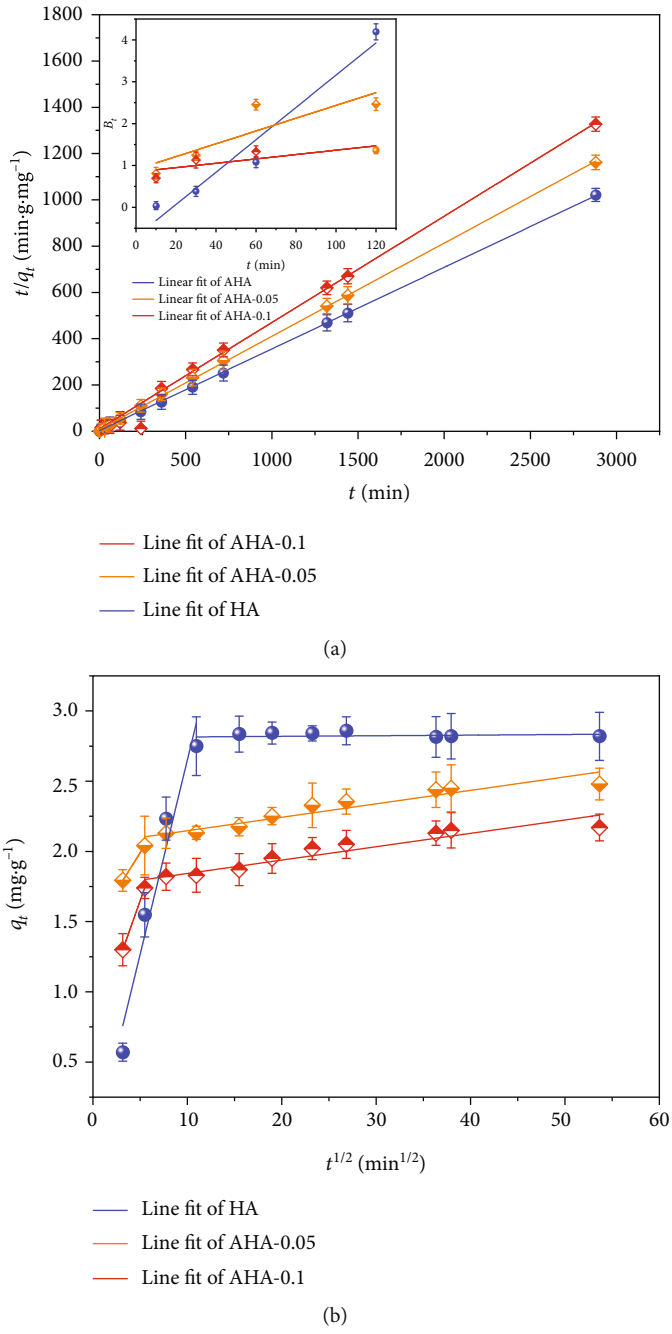

Figure 3: (a) The pseudo-second-order kinetic model fitting the adsorption of TC onto HA, AHA-0.05 and AHA-0.1, respectively (insert is the e Boyd's film-diffusion model fitting the adsorption of TC onto HA, AHA-0.05 and AHA-0.1, respectively); (b) the Weber and Morris intraparticle diffusion model fitting the adsorption of TC onto HA, AHA-0.05, and AHA-0.1, respectively.

elements. Based on SEM and EDS analysis, it can be concluded that $CaCO_3$ precipitation was successfully coated on the surface of HA to generate AHA.

3.2. Adsorption of TC over HA and AHA Samples

3.2.1. Adsorption of TC at Different Contact Times. The effect of contact time on the adsorption of TC by HA, AHA-0.05, and AHA-0.1 was evaluated (Figure 2(a)), in which AHA-0.05 and AHA-0.1 indicated the concentration of $CaCO_3$ used for wrapping HA was 0.05 mol/L and 0.1 mol/L, respectively. All the adsorption processes were divided into three stages according to the variation trend of qt along with contact time: stage 1 (0-120 min), stage 2 (120-1320 min), and stage 3 (1320-3000 min). The aforementioned three stages corresponded to a rapid increase in q_t value, a slight increase in q_t value, and an almost unchanged q_t value. The equilibrium times were determined at 1320 min, and the equilibrium adsorption capacities (q_e) of HA, AHA-0.05, and AHA-0.1 were 2.82, 2.48, and 2.17 mg/g, respectively. The

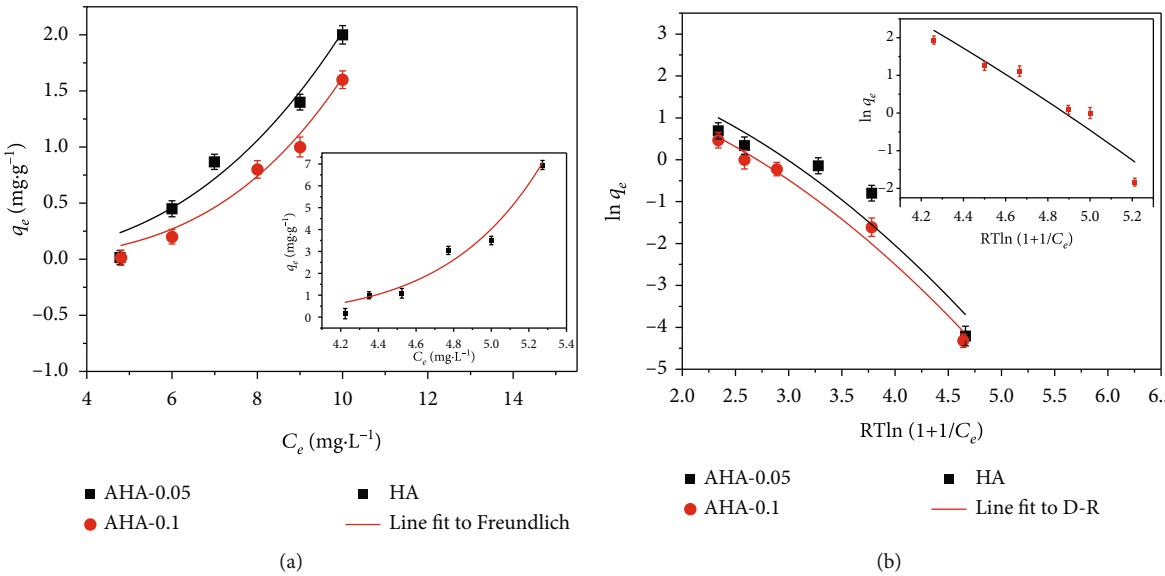

Figure 4: (a) Freundlich model fitting the adsorption of TC on the AHA-0.05 and AHA-0.1 HA, and insert is the HA; (b) Dubinin-Radushkevich model fitting the adsorption of TC on the AHA-0.05 and AHA-0.1, and insert is the HA.

removal efficiency of TC by HA at equilibrium time was more than 90%, obviously higher than it for AHA-0.05 (81%) and AHA-0.1 (71%) (the insert in Figure 2(a)).

As for stage 1 (0-120 min), the ratio of qt at 30 min to q_e for AHA-0.1 and AHA-0.05 was 0.82 and 0.84, respectively, while for HA only 0.55 (Figure 2(b)). When the contact time was prolonged to 120 min, the corresponding ratios ($q_{t120min}/q_e$) were 0.86, 0.87, and 0.98. Interestingly, the value of $q_{t120min}$ minus q_{t30min} equaled 0.43 for HA whereas less than 0.04 for the two AHA samples. These results indicated that for AHA most of the adsorption happened in the first 30 min. The possible reason was that the numbers of adsorption sites on the surface of AHA-0.1 and AHA-0.05 were less than those of HA due to the formation of $CaCO_3$ deposits. TC molecular would occupy most of the adsorption sites on the surfaces of AHA-0.1 and AHA-0.05 at the initial 30 min owing to the limited numbers in adsorption sites. Different from AHA samples, HA provided adequate adsorption sites. Therefore, TC may attach to the sites with higher energy and then the sites with lower energy, possibly resulting in a relatively slower increase in the value of q_t in the initial 30 min.

The values of q_t at different contact times for the three adsorbents were treated by using a pair-wise comparison, and the results are shown in Figure 2(c). The ratios of $q_{tAHA-0.05}/q_{tAHA-0.1}$ were almost maintained at 1.2 during the whole adsorption process from 10 to 2880 min. The ratios of $q_{tHA}/q_{tAHA-0.05}$ and $q_{tHA}/q_{tAHA-0.1}$ increased quickly from 10 to 240 min, in which the values reached the maximum at 240 min (1.3 for the former and 1.5 for the latter). From 240 to 1320 min, the ratios began to decrease and then kept unchanged from 1320 to 2880 min. As $q_{tHA}/q_{tAHA-0.05}$ multiply by $q_{tAHA-0.05}/q_{tAHA-0.1}$ equals to $q_{tHA}/q_{tAHA-0.1}$, as well as $q_{tAHA-0.05}/q_{tAHA-0.1}$ was almost fixed at 1.2, which means that the values of $q_{tHA}/q_{tAHA-0.1}$ were 1.2 times higher than those of $q_{tHA}/q_{tAHA-0.05}$ during the whole adsorption process from 0 to 2880 min. The difference between q_{tHA}/q_{tAHA} and $q_{tAHA-0.05}/q_{tAHA-0.1}$ was the biggest at 10 min and then shrank at 30 min, which further proved that most of the adsorption for AHA samples occurred in the initial stage even at the first 10 minutes.

Table 2: Parameters of the isotherm models describing the sorption of TC.

Model	Parameters	HA	AHA-0.05	AHA-0.1
D-R				
	E/kJ·Mol^{-1}	2.083	1.730	1.740
	q_D/mg·g^{-1}	33.115	13.197	8.248
	R^2	0.920	0.970	0.900
Freundlich				
	K_F/mg·L$^{-(1-1/n)}$·g^{-1}	0.016	0.003	0.0005
	n	0.296	0.340	0.381
	R^2	0.960	0.920	0.972

3.2.2. Adsorption Kinetics and Isotherm. The pseudo-first-order kinetic model and the pseudo-second-order kinetic model were used and all the parameters were listed in Table 1 and Figure 3(a). The pseudo-second-order kinetic model presented a better fit for HA, AHA-0.05, and AHA-0.1 based on the values of R^2. Furthermore, the calculated q_e values (2.841, 2.488, and 2.197 mg/g for HA, AHA-0.05, and AHA-0.1, respectively) were close to the experiment data (2.82, 2.48, and 2.17 mg/g, respectively). From Table 1, it can be seen that the value of $K_2q^2_{e,cal}$ for HA was larger than those for AHA-0.05 and AHA-0.1, indicating that the initial adsorption rate of TC by the three adsorbents followed the order of HA > AHA − 0.05 > AHA − 0.1.

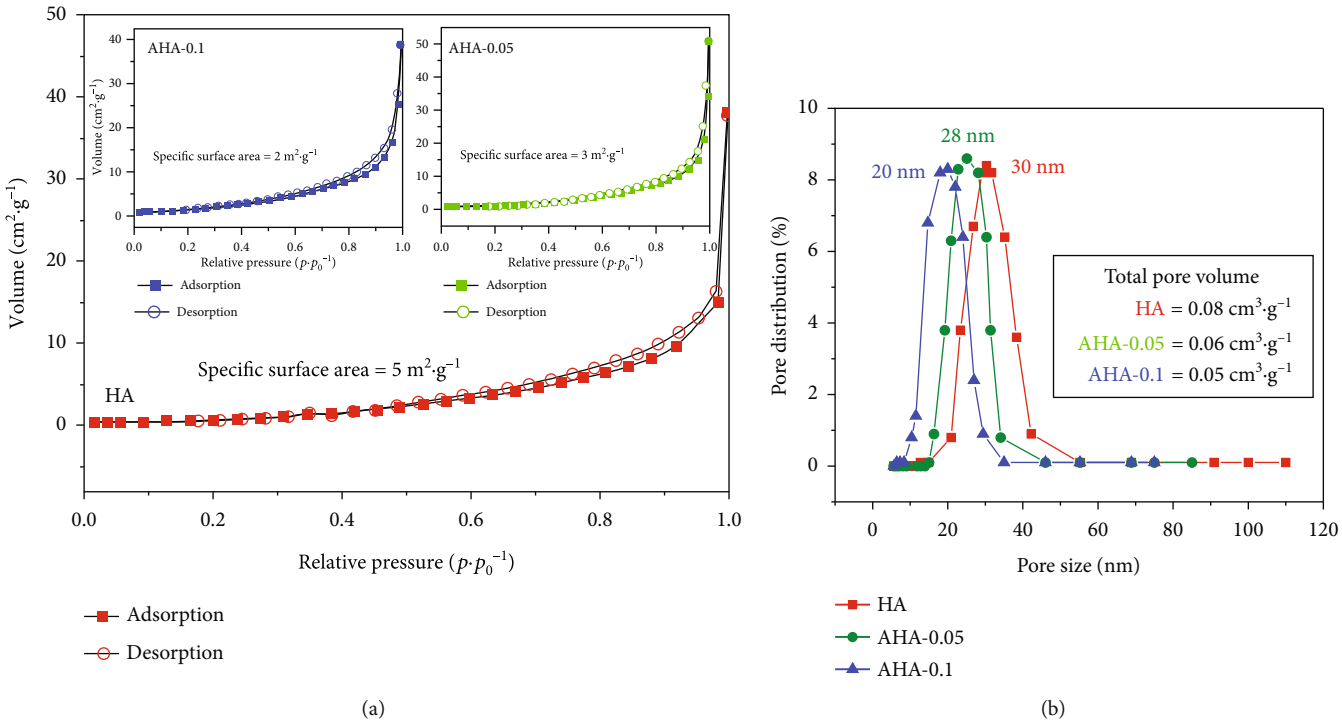

FIGURE 5: (a) Nitrogen sorption-desorption isotherm for HA, insert for AHA samples; (b) pore size distribution of HA, AHA-0.05 and AHA-0.1.

The Weber and Morris intraparticle diffusion model was used to investigate the rate-limiting step, and all the fitting dates are shown in Table 1. As shown in Figure 3(b), it was found that the fitted curves can be separated into two parts distinctly. All the first lines did not pass through the origin, suggesting that the rate-controlling step for the adsorption of TC on HA, AHA-0.05, and, AHA-0.1 proceeded by the boundary layer and intraparticle diffusion simultaneously. The diffusion coefficients of K_{id1} for HA (0.276 mg/g.h$^{1/2}$) were higher than those for AHA-0.05 (0.041 mg/g.h$^{1/2}$) and AHA-0.1(0.039 mg/g.h$^{1/2}$), indicating that the deposits of $CaCO_3$ existing on the surface of AHA reduced the mass transfer rate of TC from the aqueous liquid to the external surface of the adsorbent. Fan et al. [23] indicated that when the curve fitted by the Weber and Morris internal particle diffusion model is extended to y-axis, the intercept obtained is proportional to the thickness of the boundary layer. The larger the intercept is, the thicker the boundary layer has. In this study, the values of I_1 for HA, AHA-0.05, and AHA-0.1 were -0.115, 1.493, and 1.742 mg/g, respectively, indicating that when HA was coated with a higher concentration of calcium carbonate, more calcium carbonate precipitates accumulated on the surface of AHA.

To further determined the real control step of the adsorption process of TC. The Boyd's film diffusion model was used. Table 1 showed the results of adsorption kinetics. If the plot was nonlinear or linear but does not passes through the origin, the adsorption rate was controlled by film-diffusion. If the plot of B_t against time was linear and passed through the origin, intraparticle diffusion controls the rate of mass transfer [23]. Based on the results from Table 1 and the insert of Figure 3(a), although the plot of B_t against time was linear but the intercept of the plots of HA, AHA-0.05, and AHA-0.1, adsorption are -0.702, 0.906, and 0.845, which were significantly different from zero. The intercept of the plots of AHA was farther away from zero, and according to the result of the intro-particle diffusion plot, it is indicated that the adsorption rate of TC on AHA was more greatly affected by film diffusion.

Freundlich and D-R model fitting results are shown in Figure 4, and the fitting parameters are shown in Table 2. For the Freundlich model, the value of R^2 for HA, AHA-0.05, and AHA-0.1 was 0.960, 0.920, and 0.972, respectively, while for the Dubinin-Radushkevich model the values of R^2 were correspondingly 0.920, 0.970 and 0.900. Adsorption free energy E can be determined from the D-R isotherm, which gives information about the adsorption nature. If the magnitude of E is between 8 and 16 kJ/mol, the sorption process is chemical. If the value of E is less than 8 kJ/mol, the sorption process is supposed to proceed via physical sorption [24]. Based on Table 2, it can be concluded that the adsorption nature of the TC on HA, AHA-0.05, and AHA-0.1 was physisorption.

3.2.3. Adsorption Performance Comparison. Figure 2(d) compared the kinetic and isotherm parameters among the three adsorbents. The parameter of $K_2q^2_{e,cal}$ derived from the pseudo-second-order kinetic model represents the initial adsorption rate [19]. It can be seen that HA possessed the fastest initial adsorption rate then followed by AHA-0.05 and AHA-0.1. The diffusion coefficient of K_{id1} from the Weber and Morris intraparticle diffusion

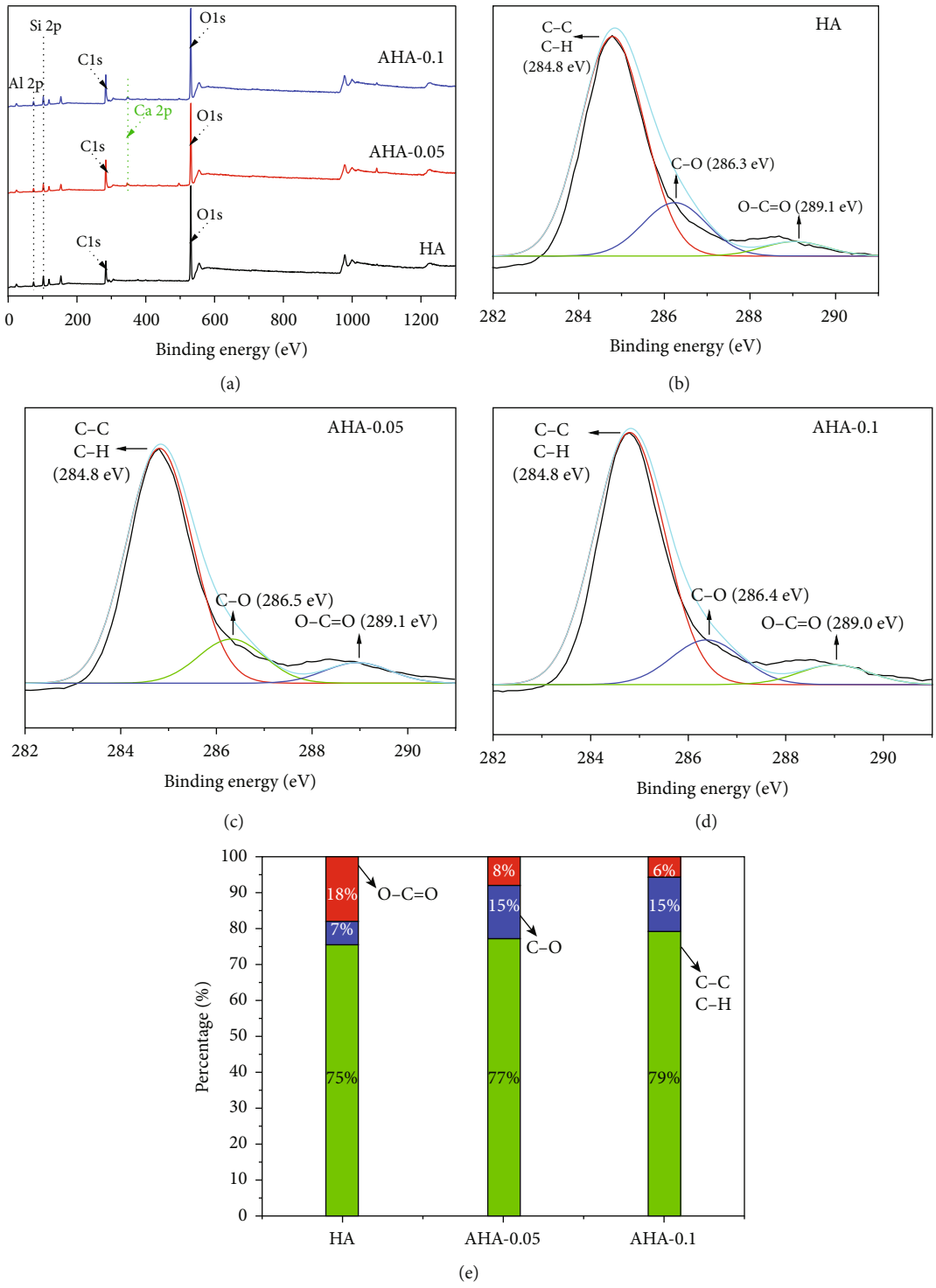

FIGURE 6: (a) XPS full scan spectra of HA and AHA samples; high resolution C1s XPS spectra of (b) HA (c) AHA-0.05, and (d) AHA-0.1; (e) the percentage of different functional groups carried by HA, AHA-0.05 and AHA-0.1.

model followed the order of HA > AHA − 0.05 > AHA − 0.1. The possible reason is that the formation of $CaCO_3$ deposits on the surface of AHA samples impeded the mass transfer of TC from solution bulk to the outer surface of the adsorbents [20]. The values of K_{id1} can also explain why the parameter of $K_2 q^2_{e,cal}$ for HA was significantly bigger than those for AHA-0.05 and AHA-0.1. Based on the values of K_F (Freundlich constant), it can be concluded that HA adsorbed more amounts of TC than AHA samples. These results demonstrated that once HA was wrapped by $CaCO_3$, the adsorption capacity towards TC decreased obviously.

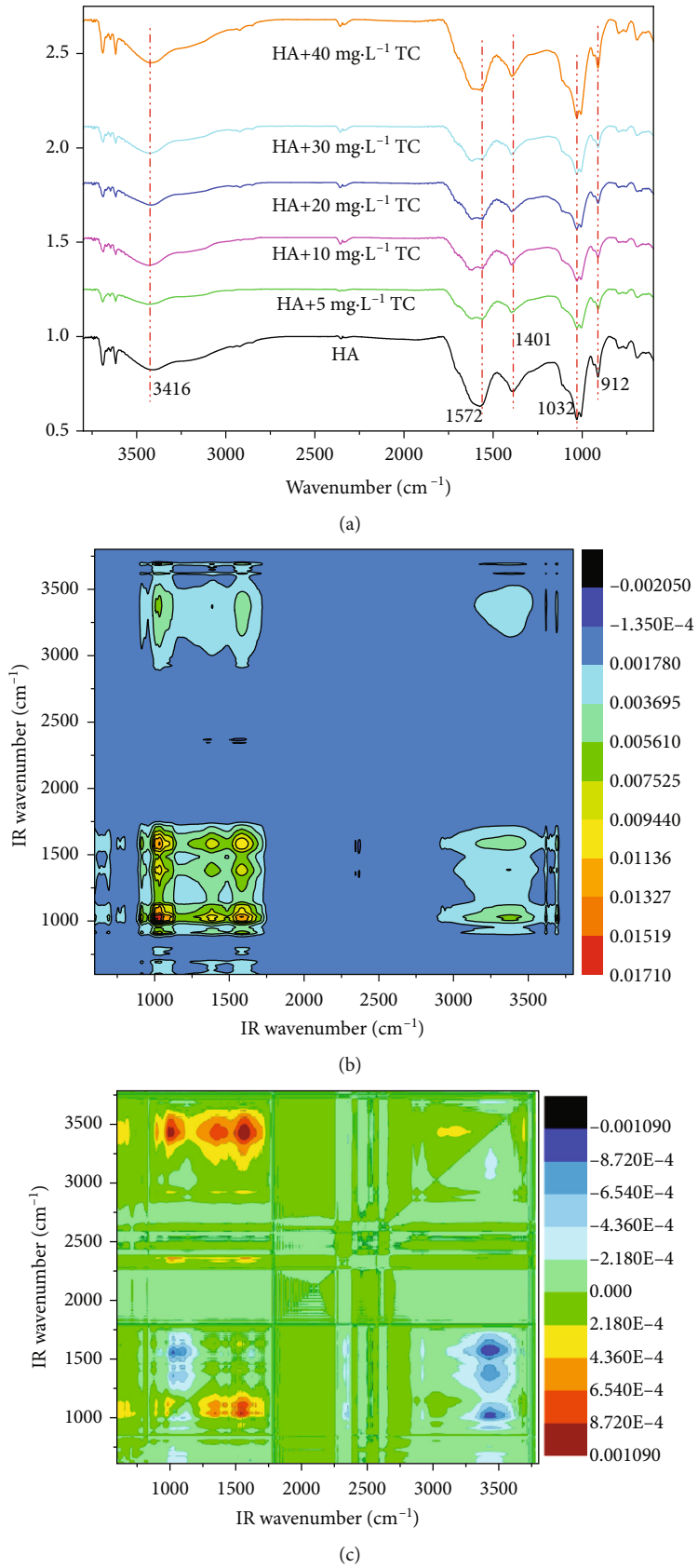

Figure 7: (a) FT-IR spectra of HA sample and HA after adsorbed different concentrations of TC; (b) synchronous and (c) asynchronous 2D correlation maps generated from the FT-IR.

3.3. Adsorption Mechanism of TC by HA and AHA Samples

3.3.1. Morphology Analysis. As shown in Figure 5(a), HA, AHA-0.05, and AHA-0.1 samples exhibited type-III adsorption isothermal curves, in which the BET specific surface areas were calculated to be 5, 3, and 2 $m^2 \cdot g^{-1}$, respectively. The correspondingly total pore volumes were 0.08, 0.06 and 0.05 $cm^3 \cdot g^{-1}$ ($P/P0 = 0.9933$) (Figure 5(b)). The decreasing percentages ($(S_{HA} - S_{AHA})/S_{HA}$) of AHA-0.05 to HA and AHA-0.1 to HA in BET specific surface areas were 44% and 50%, respectively. As can be seen from Figure 5(b), the pore sizes of the three adsorbents are mainly concentrated at 30 nm (HA), 28 nm (AHA-0.05), and 20 nm (AHA-0.1), respectively. These results demonstrated that the formation of $CaCO_3$ deposits on the surface of AHA samples rendered them with lower specific surface areas and smaller pore sizes compared to HA, which explains why the HA samples possessed quicker adsorption kinetics and higher adsorption amount.

3.3.2. Chemical Composition Analysis. In addition to the pore analysis, the morphology and the functional groups of fresh HA and aged HA were compared. The adsorption mechanisms of TC on fresh HA and aged HA were explored. The functional groups of the tree adsorbents were also analyzed by XPS technology to explain the adsorption mechanism from the viewpoint of molecular interaction. As shown in Figure 6(a), the full scan survey XPS spectra revealed that HA, AHA-0.05, and AHA-0.1 were mainly composed of C and O as well as small amounts of Si and Al. Interestingly, a new peak of Ca 2p emerged for the two AHA samples, suggesting that calcium carbonate covered their surfaces. Figures 6(b)–6(d) are the XPS high-resolution graphs of C 1 s for HA, AHA-0.05, and, AHA-0.1, in which it was found that three states of carbon existed. It is well known that the C element has four kinds of binding forms. The first one is carbon atom links with carbon or hydrogen atom to form C-C or C-H corresponding to relatively lower binding energy (285 eV) [25]. The second one is the carbon atom connects with the carbonyl oxygen atom to form C-O at 286. 5 eV. The third one is carbon atom binds with two oxygen atoms (O-C-O) or connects with one atom of oxygen to form $C = O$, in which the energy spectrum peak locate between 288~288.5 eV [26]. The last one is a carbon atom that reacts with two oxygen atoms to generate $O - C = O$ under high binding energy of 289~289.5 eV [26]. Therefore, it can be deduced that HA possessed the functional groups of C-C or C-H (284.8 eV), C-O (286.3 eV), and O-C=O bond (289.1 eV) (Figure 6(b)). Similar conclusions can be used for AHA-0.05 and AHA-0.1 (Figures 6(c) and 6(d)). Furthermore, the content of the three functional groups was calculated, and the results were given in Figure 6(e). It was observed that after being wrapped by $CaCO_3$, the percentage of $O - C = O$ for the two AHA samples decreased obviously compared to HA and followed the order of HA > AHA − 0.05 > AHA − 0.1.

The FT-IR spectra of HA before and after adsorption of TC are shown in Figure 7(a). The peak at 3416 cm^{-1} was attributed to the stretching vibration of phenolic hydroxyl or alcohol hydroxyl [27]. The peak at 1572 cm^{-1} was identified as N-H bending or C-N stretching vibration of amide II [19]. The peak at 1401 cm^{-1} belonged to the symmetric vibration of carboxylate [28]. A sharp band at 1032 cm^{-1} was assigned to C-O, which indicated the occurrence of carbohydrates [29]. The sharp peak at 912 cm^{-1} belonged to the vibration of the aliphatic skeleton [27]. 2D-COS was further used to analyze the FT-IR to sequence the binding affinity of HA towards TC. On the diagonals of the synchronization graph (Figure 7(b)), there are five self-intersecting positive peaks appeared at the main diagonal, as well as five cross-peaks were observed on both sides of the diagonal, indicating that the signal of functional groups on the surface of HA changed along with the change in TC concentrations. In the asynchronous map (Figure 7(c)), six cross-peaks located at 912/1032 cm^{-1}, 912/3416 cm^{-1}, 1032/3416 cm^{-1}, 1401/1572 cm^{-1}, 1572/3416 cm^{-1}, and 1401/3416 cm^{-1} were positive. Four negative peaks were located at 912/1401 cm^{-1}, 912/1572 cm^{-1}, 1032/1401 cm^{-1}, and 1032/1572 cm^{-1}. Table 3 lists the signs of each cross peak in the synchronous (Φ) and asynchronous (Ψ) maps. According to Noda's rule [30], it can be concluded that the sequence of the binding affinities of TC was −COO > N − H > −C − C > C − O > O − H, which means that -COO was the most sensitive group.

Table 3: Signs of each cross peak in the synchronous (Φ) and asynchronous (Ψ) maps.

Position (cm^{-1})	Sign				
	912	1032	1401	1572	3416
912	+	+	—	—	+
1032		+	—	—	+
1401			+	+	+
1572				+	+
3416					+

(signs were obtained in the maps of 2D-COS map, + positive and - negative).

The analysis result from XPS (Figure 6(e)) proved that the content of -COO decreased once HA was wrapped by $CaCO_3$ deposits, in which it followed the order of HA > AHA − 0.05 > AHA − 0.1. As FTIR-2D-COS indicates that -COO was the functional group with the highest affinity towards TC, it explains why HA possessed the biggest adsorption amounts and fastest adsorption kinetics and then followed by AHA-0.05 and AHA-0.1 (Figure 2(d)).

4. Conclusions

The adsorption capacities of TC by HA, AHA-0.05, and AHA-0.1 were evaluated, in which AHA-0.05 and AHA-0.1 indicated that HA was wrapped by 0.05 mol/L and 0.1 mol/L of $CaCO_3$, respectively. The initial adsorption rate ($K_2 q^2_{e,cal}$) for HA was calculated to be 0.299 mg/(g h), while for AHA-0.05 and AHA-0.1 were 0.125 and 0.096 mg/(g h). The values of diffusion coefficient K_{id1} were 0.276, 0.041, and 0.039 mg/(g·$h^{1/2}$) corresponding to HA, AHA-0.05, and AHA-0.1. Freundlich constant K_F for HA, AHA-0.05, and AHA-0.1 was 0.016, 0.003, and 0.0005 mg/($L^{1-1/n}$·g),

respectively. These results suggested that HA adsorbed more amount of TC at a quicker speed than AHA samples did, demonstrating HA exhibited better adsorption performance towards TC. To explain the aforementioned phenomenon, technologies of BET, XPS, FT-IR, and 2D-COS were adopted. It was found that the specific surface areas of HA, AHA-0.05, and AHA-0.1 were 5, 3, and 2 $m^2 \cdot g^{-1}$, respectively. The functional groups of phenolic or alcohol, amide II, carboxylate group, carbohydrates, and aliphatic skeleton carried by HA were proved to be the adsorption sites for extracting TC from aqueous solution. The binding affinity of these groups towards TC was sequenced as $-COO > N-H > -C-C > C-O > O-H$, suggesting that the carboxylate group played a significant role in the adsorption of TC. The content of the carboxylate group shrunk once HA was wrapped by $CaCO_3$. As AHA samples simulated the aging process, these results demonstrated that aging will affect the physical morphology and chemical composition of HA itself and consequently lead to the decrease in the retention extent of TC in HA.

Data Availability

No data were used to support this study.

Conflicts of Interest

The authors declare that they have no known competing financial interests or personal relationships that could have appeared to influence the work reported in this paper.

Authors' Contributions

Chunli Zheng was responsible for the data curation and writing the original manuscript, reviewing, and editing. Fei He was assigned for writing the original manuscript and visualization. Zhiwu Cao was tasked for the formal analysis. Xingxing Cheng was charged for writing the original manuscript. Zhenxing Wang was responsible for the conceptualization and funding acquisition.

Acknowledgments

This work was funded by National Key Research and Development Project (2019YFC1804800); Key R&D Program of Shaanxi Province (2019SF-253); the Fundamental Research Funds for the Central Universities, CHD (300102291504); the Pearl River S&T Nova Program of Guangzhou, China (201710010065); the Science and Technology Program of Guangdong Forestry Administration (2020-KYXM-08), and the Key Laboratory of Resource Chemistry, Ministry of Education (KLRC_ME2102). We are very thankful for the support of the Instrument Analysis Center of Xi'an Jiaotong University.

Supplementary Materials

Description about the graphical abstract: the methodology of coating $CaCO_3$ precipitation on the surface of HA was adopted to simulate the aging process. It was found that aging resulted in the decrease in BET specific area and pore size of humic acid and aging negatively affected the content of the COO- group carried by humic acid. *(Supplementary Materials)*

References

[1] S. W. Zhou, Y. B. Ma, and M. G. Xu, "Ageing of added copper in bentonite without and with humic acid," *Chemical Speciation and Bioavailability*, vol. 21, no. 3, pp. 175–184, 2009.

[2] Q. Q. Zhang, G. G. Ying, C. G. Pan, Y. S. Liu, and J. L. Zhao, "Comprehensive evaluation of antibiotics emission and fate in the river basins of China: source analysis, multimedia modeling, and linkage to bacterial resistance," *Environmental Science & Technology*, vol. 49, no. 11, pp. 6772–6782, 2015.

[3] P. Wang and A. A. Keller, "Sorption and desorption of atrazine and diuron onto water dispersible soil primary size fractions," *Water Research*, vol. 43, no. 5, pp. 1448–1456, 2009.

[4] A. Delle Site, "Factors affecting sorption of organic compounds in natural sorbent/water systems and sorption coefficients for selected pollutants. A review," *Journal of Physical and Chemical Reference Data*, vol. 30, no. 1, pp. 187–439, 2001.

[5] S. U. Khan, "Distribution and characteristics of organic matter extracted from the black solonetzic and black chernozemic soils of Alberta: the humic acid fraction," *Soil Science*, vol. 112, no. 6, pp. 401–409, 1971.

[6] S. Vaz Jr., W. T. Lopes, and L. Martin-Neto, "Study of molecular interactions between humic acid from Brazilian soil and the antibiotic oxytetracycline," *Environmental Technology & Innovation*, vol. 4, pp. 260–267, 2015.

[7] C. Gu, K. G. Karthikeyan, S. D. Sibley, and J. A. Pedersen, "Complexation of the antibiotic tetracycline with humic acid," *Chemosphere*, vol. 66, no. 8, pp. 1494–1501, 2007.

[8] V. Maryganova, L. W. Szajdak, and L. Tychinskaya, "Hydrophobic and hydrophilic properties of humic acids from soils under shelterbelts of different ages," *Chemistry and Ecology*, vol. 26, no. sup2, pp. 25–33, 2010.

[9] Y. Yu, Y. A. Wan, A. Y. Camara, and H. F. Li, "Effects of the addition and aging of humic acid-based amendments on the solubility of cd in soil solution and its accumulation in rice," *Chemosphere*, vol. 196, pp. 303–310, 2018.

[10] J. B. Regitano, W. C. Koskinen, and M. J. Sadowsky, "Influence of soil aging on sorption and bioavailability of simazine," *Journal of Agricultural and Food Chemistry*, vol. 54, no. 4, pp. 1373–1379, 2006.

[11] Q. Zhao, P. J. Li, F. Stagnitti et al., "Effects of aging and freeze-thawing on extractability of pyrene in soil," *Chemosphere*, vol. 76, no. 4, pp. 447–452, 2009.

[12] Q. Zhao, B. S. Xing, P. D. Tai et al., "Effect of freeze-thawing cycles on soil aging behavior of individually spiked phenanthrene and pyrene at different concentrations," *Sci Total Environ*, vol. 444, pp. 311–319, 2013.

[13] J. H. See and D. A. Bronk, "Changes in C:N ratios and chemical structures of estuarine humic substances during aging," *Marine Chemistry*, vol. 97, no. 3-4, pp. 334–346, 2005.

[14] W. R. Reeves, T. J. McDonald, N. R. Bordelon, S. E. George, and K. C. Donnelly, "Impacts of aging on in vivo and in vitro measurements of soil-bound polycyclic aromatic hydrocarbon availability," *Environmental Science & Technology*, vol. 35, no. 8, pp. 1637–1643, 2001.

[15] N. E. Guthrie, A. Grasham, C. Kazunga et al., "The effect of aging on pyrene transformation in sediments," *Environmental Toxicology and Chemistry*, vol. 22, no. 1, pp. 40–49, 2003.

[16] X. J. An, B. H. Xiao, X. Y. Di, H. Dong, H. M. Tang, and S. S. Wu, "Effect of inorganic ion precipitation on hydrophobic organic pollutant adsorption by non-extracted soil organic matters," *Earth Environment (In Chinese)*, vol. 44, no. 5, pp. 572–580, 2016.

[17] B. Pan, B. S. Xing, S. Tao et al., "Effect of physical forms of soil organic matter on phenanthrene sorption," *Chemosphere*, vol. 68, no. 7, pp. 1262–1269, 2007.

[18] A. K. Sarmah, M. T. Meyer, and A. B. A. Boxall, "A global perspective on the use, sales, exposure pathways, occurrence, fate and effects of veterinary antibiotics (VAs) in the environment," *Chemosphere*, vol. 65, no. 5, pp. 725–759, 2006.

[19] X. X. Cheng, H. B. Hou, R. S. Li, C. L. Zheng, and H. X. Liu, "Adsorption behavior of tetracycline on the soil and molecular insight into the effect of dissolved organic matter on the adsorption," *Journal of Soils and Sediments*, vol. 20, no. 4, pp. 1846–1857, 2020.

[20] P. P. Liu, Q. R. Wang, C. L. Zheng, and C. He, "Sorption of sulfadiazine, norfloxacin, metronidazole, and tetracycline by granular activated carbon: kinetics, mechanisms, and isotherms," *Water, Air, & Soil Pollution*, vol. 228, no. 4, p. 129, 2017.

[21] X. X. Cheng, C. L. Zheng, Q. Lu et al., "Adsorption of furazolidone, D-cycloserine, and chloramphenicol on granular activated carbon made from corn stover," *Journal of Environmental Engineering*, vol. 145, no. 7, article 04019038, 2019.

[22] Y. R. Fan, C. L. Zheng, A. D. Huo et al., "Investigating the binding properties between antimony (V) and dissolved organic matter (DOM) under different pH conditions during the soil sorption process using fluorescence and FTIR spectroscopy," *Ecotoxicology and Environmental Safety*, vol. 181, pp. 34–42, 2019.

[23] Y. R. Fan, C. L. Zheng, Z. S. Lin, A. D. Huo, R. S. Li, and C. He, "Influence of sulfamethazine (smt) on the adsorption of antimony by the black soil: implication for the complexation between smt and antimony," *Science of The Total Environment*, vol. 760, article 143318, 2021.

[24] M. J. Ahmed and S. K. Theydan, "Microporous activated carbon from _Siris_ seed pods by microwave-induced KOH activation for metronidazole adsorption," *Journal of Analytical and Applied Pyrolysis*, vol. 99, pp. 101–109, 2013.

[25] G. Sinn, A. Reiterer, and S. E. Stanzl-Tschegg, "Surface analysis of different wood species using X-ray photoelectron spectroscopy (XPS)," *Journal of Materials Science*, vol. 36, no. 19, pp. 4673–4680, 2001.

[26] L. Todaro, M. D'Auria, F. Langerame, A. M. Salvi, and A. Scopa, "Surface characterization of untreated and hydrothermally pre-treated Turkey oak woods after UV-C irradiation," *Surface and Interface Analysis*, vol. 47, no. 2, pp. 206–215, 2015.

[27] Z. M. Gu, X. R. Wang, X. Y. Gu, and X. D. Cao, "Characterization of humic acid extracted from different soils by Fourier transform infrared spectrometry and nuclear magnetic resonance," *Chinese Journal of Analytical Chemistry (In Chinese)*, vol. 28, no. 3, pp. 314–317, 2000.

[28] N. Li, J. G. Wu, and H. F. Xia, "Study on humic acids of the soil applied with corn plant residue by Fourier transform infrared spectroscopy," *Plant Nutrition and Fertilizer Science*, vol. 13, no. 5, pp. 974–978, 2007.

[29] Y. F. Wang, X. Y. Zhang, X. Zhang, Q. J. Meng, F. J. Gao, and Y. Zhang, "Characterization of spectral responses of dissolved organic matter (DOM) for atrazine binding during the sorption process onto black soil," *Chemosphere*, vol. 180, pp. 531–539, 2017.

[30] I. Noda, Y. L. Liu, Y. Ozaki, and M. A. Czarnecki, "Two-dimensional Fourier transform near-infrared correlation spectroscopy studies of temperature-dependent spectral variations of Oleyl alcohol," *The Journal of Physical Chemistry. B*, vol. 99, no. 10, pp. 3068–3073, 1995.